Targeted Generation of DNA Strand Breaks Using Pyrene-Conjugated Triplex-Forming Oligonucleotides[†]

Aaron P. Benfield,[‡] Michael C. Macleod,[‡] Yaobin Liu,[‡] Qi Wu,[‡] Theodore G. Wensel,[§] and Karen M. Vasquez*,[‡]

Department of Carcinogenesis, The University of Texas M. D. Anderson Cancer Center, Science Park-Research Division, Smithville, Texas 78957, and Department of Biochemistry, Baylor College of Medicine, Houston, Texas 77380

Received December 7, 2007; Revised Manuscript Received March 20, 2008

ABSTRACT: Gene targeting by triplex-forming oligonucleotides (TFOs) has proven useful for gene modulation *in vivo*. Photoreactive molecules have been conjugated to TFOs to direct sequence-specific damage in double-stranded DNA. However, the photoproducts are often repaired efficiently in cells. This limitation has led to the search for sequence-specific photoreactive reagents that can produce more genotoxic lesions. Here we demonstrate that photoactivated pyrene-conjugated TFOs (pyr-TFOs) induce DNA strand breaks near the pyrene moiety with remarkably high efficiency and also produce covalent pyrene-DNA adducts. Free radical scavenging experiments demonstrated a role for singlet oxygen activated by the singlet excited state of pyrene in the mechanism of pyr-TFO-induced DNA damage. In cultured mammalian cells, the effect of photoactivated pyr-TFO-directed DNA damage was to induce mutations, in the form of deletions, ~7-fold over background levels, at the targeted site. Thus, pyr-TFOs represent a potentially powerful new tool for directing DNA strand breaks to specific chromosomal locations for biotechnological and potential clinical applications.

Triplex-forming oligonucleotides (TFOs)[1] have been employed to modulate gene structure and function, both *in vitro* and *in vivo*. When conjugated to DNA damaging agents, TFOs can induce site-directed DNA damage resulting in enhanced mutagenesis and recombination (reviewed in refs *1*–*8*). Reactive molecules that have been conjugated to TFOs include, but are not limited to, 2-amino-6-vinylpurine, haloacetyl amide, aryl nitrogen mustard, N^4,N^4-etheno-5-methyldeoxycytidine, and various psoralen derivatives. All of these induce site-specific cross-linking and/or alkylation in double-stranded DNA (dsDNA) (*9*–*15*). Psoralen-linked TFOs (pso-TFOs), which can induce covalent monoadducts on one strand or cross-links with both strands of duplex DNA with high efficiency and sequence specificity, are the most studied of the photoreactive TFOs. Pso-TFOs can yield site-specific DNA damage with high efficiency and have been used to introduce mutations and inactivate target genes. However, the existence of cellular mechanisms for repairing the pso-TFO photoproducts without introduction of sequence errors has limited their utility.

Recent efforts by several groups have improved the binding affinity and sequence specificity of TFOs *in vivo*. For example, Puri and colleagues found that 2′-*O*-aminoethyl (2′-AE) ribose substitutions within pso-TFOs increased triplex stability and targeted gene inactivation frequencies of a chromosomally integrated hypoxanthine guanine ribosyl transferase gene (*16, 17*). The bioactivity of 2′-AE-substituted pso-TFOs is most efficient during S-phase when adducts can be induced in ~30% of targeted sequences within chromatin (*18*). In the latter scenario ~75% of those adducts were resolved in an error-free fashion, resulting in an overall mutation frequency of ~7%, 95% of which were single base substitutions.

While recent work has improved TFO specificity and affinity for sequences within chromosomal DNA in cells, and TFO-targeted gene in activation has been achieved in mice (*19*), higher efficiency TFO-directed gene modification is needed to make this an attractive approach for clinical purposes and to improve its value as an experimental tool. One of the most promising approaches for enhancing TFO-directed DNA damage is the introduction of TFOs conjugated with photoreactive species capable of inducing DNA double-strand breaks (DSBs). While single-strand DNA breaks are repaired with high efficiency, DNA DSBs are more difficult to repair and, if left unrepaired, are highly lethal to cells. ^{125}I-labeled TFOs (I-TFOs) (*20*–*22*) and TFOs conjugated to nonspecific nucleases (nnu-TFOs) (*23*), restriction enzymes (rez-TFOs) (*24*), and EDTA (EDTA-TFOs) (*25*) all can induce DNA DSBs on targeted sequences. However, the potential for these TFOs to induce DSBs is either limited to special conditions, such as the requirement for a reducing environment and Fe(II) for EDTA-TFOs, the need for a specific sequence adjacent to the targeted sequence for rez-TFOs, or a lack of specificity in the case of I-TFOs and nnu-

[†] Funding was provided in part from the National Institutes of Health (CA93729 to K.M.V.) and the National Institute of Environmental Health Sciences (ES007784).

* To whom correspondence should be addressed: e-mail, kvasquez@mdanderson.org; phone, 512-237-9324; fax, 512-237-2475.

[‡] The University of Texas M. D. Anderson Cancer Center.

[§] Baylor College of Medicine.

[1] Abbreviations: *Aprt*, adenine phosphoribosyl transferase; DMF, dimethylformamide; DSB, double-strand break; dsDNA, double-stranded DNA; EMSA, electrophoretic mobility shift assay; HMWC, high molecular weight complex; PAH, polycyclic aromatic hydrocarbon; pso-, psoralen; pyr-, pyrene; SBs, strand breaks; TFO, triplex-forming oligonucleotide.

10.1021/bi7024029 CCC: $40.75
Published on Web 05/13/2008

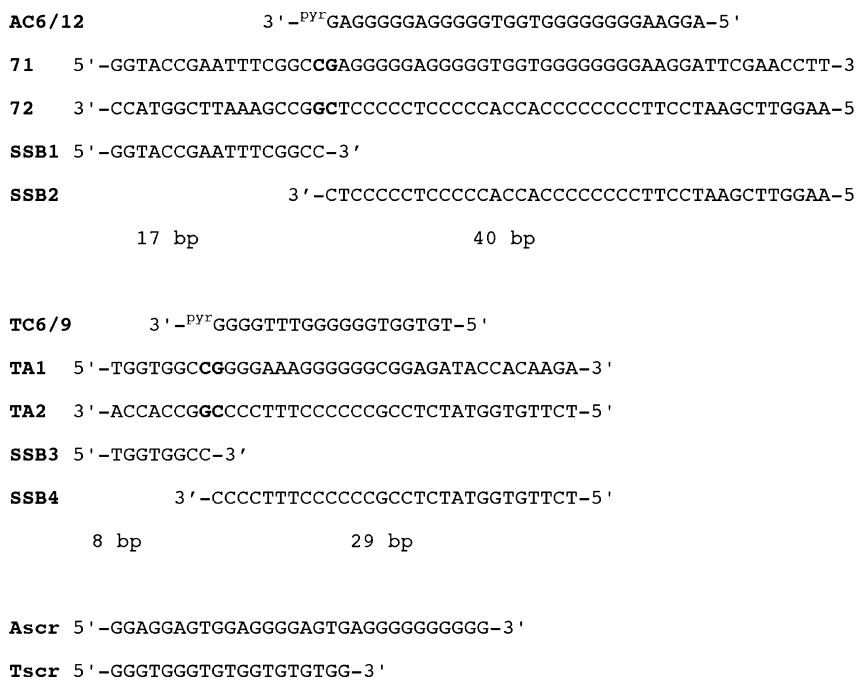

FIGURE 1: TFOs and substrates used in this study. TFOs, AC6 and AC12, are specific for the *supF* duplex substrate 71/72, whereas TC6 and TC9 bind to the *Aprt* target duplex, TA1/TA2. Ascr and Tscr contain the same nucleic acid composition as the specific TFOs but are scrambled versions of AC6/AC12 and TC6/TC9, respectively. Oligonucleotides SSB1, SSB2, SSB3, and SSB4 were used as markers for the products resulting from pyr-TFO-induced strand cleavage of 71, 72, TA1, and TA2, respectively.

TFOs. Unlike photoreactive TFOs, I-TFOs, nnu-TFOs, rez-TFOs, and EDTA-TFOs lack the means for selectable activation.

There are only two reports of TFOs conjugated to photoreactive molecules that induce DSBs without the aid of special conditions; ellipticine-TFOs (*26*) and more recently quinacridine-TFOs (*27*). The efficiency of cutting in those cases was low and was widely distributed over the vicinity of the TFO binding sites. It has not been demonstrated previously that quinacridine or ellipticine TFO-targeted photodamage can be used to induce mutagenesis. A study employing ^{125}I-labeled TFOs to induce DSBs in cells reported mutation frequencies 7-fold greater than those obtained with pso-TFOs (*20*). Thus, additional photoreactive molecules which can be conjugated to TFOs and induce site-specific DSBs are of great interest. A promising candidate is pyrene, a polycyclic aromatic hydrocarbon (PAH). Pyrene compounds, such as benzo[*a*]pyrene (BaP) and 1-hydroxypyrene, induce DSBs as well as 8-oxo-7,8-dihydro-2′-deoxyguanosine adduct formation (*28–36*). Moreover, upon UVA (355 nm) irradiation of double-stranded pyrene-substituted oligonucleotides within duplex DNA, DSBs within ~5−7 bp of the substituted pyrene are induced at efficiencies of up to 50% (*37, 38*). Because TFOs can be targeted to specific sequences and pyrene induces both adduct formation and DSBs, we hypothesized that pyrene-conjugated TFOs (pyr-TFOs) can be used to inflict sequence-specific DNA damage in the form of DNA strand breaks and adducts.

Here, we describe the use of pyr-TFOs as a means to direct site-specific DNA damage and the use of chemical quenchers and scavengers to probe the mechanisms of damage induced by pyr-TFOs. Analysis of mutation frequencies and spectra arising from *in vivo* mammalian replication and repair of plasmid DNA containing pyr-TFO-induced DNA damage reveals the potential of this approach for site-specific manipulation of genomes.

EXPERIMENTAL PROCEDURES

Buffers. All buffers listed were tested for pH at 25 °C. TBB: 10% glycerol, 10 mM Tris base-HCl, pH 7.6, and 10 mM $MgCl_2$. TBE: 89 mM Tris base, 8.9 mM boric acid, and 1 mM EDTA at pH 8.0. TBM: 90 mM Tris base, 45 mM boric acid, and 10 mM $MgCl_2$, pH 7.6. PCB: 50 mM sodium carbonate-HCl, pH 9.0. PSB: 10 mM Tris base-HCl, pH 7.5. Denaturing gel loading buffer: 4 M urea, 2 mM Tris-HCl base, pH 7.5, 20 mM EDTA, 0.25% (m/v) xylene cyanol, and 0.25% (m/v) bromophenol blue.

Oligonucleotides. Oligonucleotides were obtained from Sigma-Genosys (The Woodlands, TX) or The Midland Certified Reagent Co., Inc. (Midland, TX). TFOs used for this study were derived from AG30, SCR30, TFO1, and TFOc (*14, 19, 39–42*) and include AG30-C6 (AC6), AG30-C12 (AC12), SCR30-C6 (Ascr), TFO1-C6 (TC6), TFO1-C9 (TC9), and TFOc-C6 (Tscr) (Figure 1). TFOs were synthesized to contain 3′ primary amine groups conjugated to TFOs via carbon linkers of differing lengths and are denoted above as C6: $CH_2CHCH_2OH(CH_2)_4NH_2$; C9: $(CH_2)_3PO_4CH_2CHCH_2OH(CH_2)_4NH_2$; C12: $[(CH_2)_3PO_4]_2$, $CH_2CHCH_2OH(CH_2)_4NH_2$. TFOs, AC6 and AC12, bind specifically to a region within the bacterial *supF* gene, whereas TC6 and TC9 specifically bind to a site within intron 1 of the hamster *Aprt* gene. TFOs Ascr and Tscr are scrambled versions of AC6 and TC6, respectively, but otherwise have the same base composition and length. For simplicity, TFO target duplex substrates used in the current study are denoted as TA1/TA2 and 71/72 and represent the targeted regions within *Aprt* and *supF*, respectively (Figure 1). Oligonucleotides SSB1, SSB2, SSB3, and SSB4 were

used as markers for the products resulting from pyr-TFO-induced strand cleavage of 71, 72, TA1, and TA2, respectively (Figure 3C).

Preparation of Pyr-TFOs. For the preparation of pyrene-conjugated TFOs (pyr-TC6, pyr-TC9, pyr-Tscr, pyr-AC6, pyr-AC12, and pyr-Ascr), 1-pyrenebutanoic acid succinimidyl ester (Invitrogen, Carlsbad, CA) was conjugated to the 3′-NH_2 ends of the TFOs using the following procedure: TFOs (2.5 nmol) were diluted with nuclease-free water (0.3 mL) in a 15 mL polypropylene tube. Following the addition of PCB (0.05 mL), 0.45 mL of pyrene solution [1 mg/mL 1-pyrenebutanoic acid succinimidyl ester in dimethylformamide (DMF)] was added to the mixture. Next, the mixture was incubated at 37 °C for 15 h in a shaker (225 rpm). The reaction was stopped with the addition of 0.3 mL of PSB. Pyr-TFOs were desalted on a Nap-5 column (GE Healthcare, Buckinghamshire, U.K.) preequilibrated with PSB and concentrated to approximately 0.05 mL using a YM-3 centrifugal filter device (Millipore, Billerica, MA). An equal volume of denaturing gel loading buffer was added, and samples were heated at 90 °C for 10 min and then subjected to denaturing PAGE (15% acrylamide and 8 M urea in TBE at 40 W for 3 h). Gels were soaked in TBE containing 10000-fold diluted Sybr-Gold (Invitrogen, Carlsbad, CA) and visualized under UV light at 254 nm. Pyrene-modified TFOs were identified as the slower migrating band in the gel, excised, and electroeluted using a Centrilutor Micro-Electroeluter (Millipore, Billerica, MA) in TBE. The purified pyr-TFOs were concentrated to approximately 1 μM. To remove trace nuclease activity, TFOs were extracted with phenol/chloroform. Overall yields for pyr-TFO formation typically ranged from 50% to 90%. Purity was assessed by UV spectroscopy and determined to be in excess of 90%. All procedures for the synthesis and purification of pyr-TFOs were carried out in the dark.

Labeling. All oligonucleotides (1−3 pmol) were labeled on their 5′ ends with [γ-^{32}P]ATP using T4 polynucleotide kinase (N.E. Biolabs, Ipswich, MA). Labeled oligonucleotides were purified by PAGE to ensure high purity prior to duplex and triplex formation. Selective labeling of oligonucleotides destined for duplex formation allowed for the purification of double-labeled duplexes (71*/72* and TA1*/TA2*) and single strand labeled duplexes (71*/72 and 71/72*), where the asterisk denotes the labeled strand. For one set of experiments pyr-TC6 was 5′-end labeled, creating pyr-TC6*.

DNA Duplex Substrate Preparation. Following labeling, pairs of complementary oligonucleotides (∼1 pmol each of 71 and 72 or of TA1 and TA2) were added to a 1.5 mL polypropylene tube. Volume and NaCl concentration were adjusted to 50 μL and 25 mM, respectively, and the mixture was heated at 90 °C for 30 min. After the samples had been allowed to cool slowly to room temperature, gel loading buffer (Bio-Rad, Hercules, CA) was added, and samples were subjected to native PAGE (12% acrylamide in TBM, 2 h at 90 V). Following exposure to BioMax XAR film (Kodak, Rochester, NY) the bands containing double-stranded substrate (71/72 and TA1/TA2) were excised, electroeluted, and concentrated to 10 nM.

K_{app} Determination. Apparent binding constants (K_{app}) for the interaction of the TFOs with their target duplexes were determined by electrophoretic mobility shift assays (EMSAs) [as previously described (*41*)]. These assays were performed in TBB, and the concentration of the substrate remained constant at 0.1 nM, while TFO or pyr-TFO was adjusted to final concentrations ranging from 1×10^{-10} M to 1×10^{-7} M. Following incubation at 37 °C for at least 15 h to ensure binding equilibrium, samples were separated by native PAGE (12% acrylamide in TBM, 2 h at 90 V). Gels were dried, exposed to a Phosphor Screen (Molecular Dynamics/GE Healthcare) overnight, and scanned using a Typhoon 9410 (GE Healthcare). Bands representing triplex and duplex were quantified (ImageQuant TL, GE Healthcare) to determine the percentage of triplex formation at the corresponding concentration of TFO/pyr-TFO and used as input to Prism software (GraphPad Software, San Diego, CA) for determination of K_{app}.

Photoreaction. Samples (30 μL) contained 2 nM 71/72 or TA1/TA2 duplex substrate, 10−100 nM TFO or pyr-TFO, in TBB. After incubation at 37 °C for at least 15 h, 10 μL of each sample was irradiated for times ranging from 20 s to 5 min. The light source used was a Continuum Nd:YAG SL1 1 kW pulsed laser (Santa Clara, CA) which produced 4−6 ns pulses at a frequency of 10 Hz. The frequency-tripled output at 355 nm was 0.7−1.4 J/s, and the beam area was approximately 0.8 cm^2. Samples were manually placed as a drop on glass coverslips at the center of the beam for varying times; the incident energy specified is expressed as the energy (Joules) delivered by the entire beam during the given exposure period. The sample size was such that about one-third of the area of the beam impinged upon the sample. For sample analysis, an equal volume of denaturing gel loading buffer was added to irradiated and nonirradiated samples. Samples were then heated at 90 °C for 10 min, cooled, and applied to a denaturing gel containing 12% acrylamide and 8 M urea to separate the products by electrophoresis (50 W, 1 h, 45 min). After the gels were dried and exposed to a Phosphor screen, the bands were quantified as described above. The remaining 10 μL from each mixture was subjected to native PAGE to assay for efficiency of triplex formation. The kinetics of photobleaching and formation of strand breaks were analyzed by fitting to one- or two-exponential functions, using the nonlinear least-squares fitting routines in Origin.

Mutagenesis Assay. The mutation-reporter shuttle vector, pSupFG1 (60 nM), which contains an AC6 binding site within the *supF* reporter gene, was incubated with or without 100 nM pyr-AC6 or pyr-Ascr in TBB (20 μL total volume). Half of each sample was irradiated for 2 min (1.4 J/s at 355 nm), irradiated and nonirradiated samples were immediately transfected into mammalian COS-7 cells via electroporation (DNA Projects, Seattle, WA). After 72 h, the plasmids were extracted, purified, and digested with *Dpn*I to remove plasmids that had not replicated in the mammalian cells. The purified plasmids were then transfected into *Escherichia coli* strain MBM7070 and grown overnight at 37 °C on LB agar supplemented with 140 mg/L 5-bromo-4-chloro-3-indoyl-β-D-galactoside (X-Gal), 200 mg/L ampicillin, and 200 mg/L isopropyl β-D-thiogalactoside (IPTG). The number of white colonies (mutants) were counted and divided by the total number of blue (wild-type) and white colonies to calculate the mutation frequency. At least 35000 colonies from each sample were counted from a total of three experiments. A

Table 1: Apparent Binding Constants (K_{app}, Molar Concentration) of TFOs to Their Target Duplexes

	K_{app}[a]	K_{app}[b]
AC6	10.3×10^{-9}	11.0×10^{-9}
AC12	5.3×10^{-9}	9.9×10^{-9}
Asc	$\geq 1 \times 10^{-6}$	$\sim 5 \times 10^{-6}$
TC6	7.1×10^{-9}	8.6×10^{-9}
TC9	5.4×10^{-9}	9.2×10^{-9}
Tsc	$\geq 1 \times 10^{-6}$	$\sim 5 \times 10^{-6}$

[a] Nonconjugated TFOs. [b] Pyrene-conjugated TFOs. Errors were ±1−3 nM.

total of nine mutants (three from each experimental condition) were expanded and sequenced to determine the mutation spectra.

RESULTS

Pyrene-Conjugated TFOs Show High Affinity and Specificity for Targeted Duplexes. Two TFOs targeting specific sequences within the hamster *Aprt* and bacterial *supF* genes (*14, 19, 39–42*) were employed. These had different carbon linker lengths on their 3′ ends, conjugated here to a single pyrene moiety (Figure 1). For binding assays, pyrene-conjugated and nonconjugated TFOs were incubated with their corresponding duplex target substrates, and the apparent equilibrium dissociation constants (K_{app}) were estimated using electrophoretic gel mobility shift assays (Supporting Information Figure 1 and Table 1). For AC6, AC12, TC6, TC9, pyr-AC6, pyr-AC12, pyr-TC6, and pyr-TC9, which differ in having linker lengths between 6 and 12 carbons and in the presence or absence of pyrene, the K_{app}s were all determined to be in the range of 5−11 nM. Thus, neither the linker length nor the attachment of pyrene to the 3′ ends has a large effect on affinities of the TFOs for their target duplexes. As expected, scrambled TFO sequences and their respective pyrene conjugates (pyr-Ascr and pyr-Tscr) did not exhibit detectable binding at or below concentrations of 100 nM. However, some binding of pyr-Tscr and pyr-Ascr was observed at 5 μM (ranging between ~20% and 50%; data not shown). Thus, the scrambled pyr-TFOs exhibit binding affinities approximately 3 orders of magnitude lower than those of the TFOs specifically designed for substrates 71/72 and TA1/TA2.

Irradiation of Pyr-TFOs Induces DNA Strand Breaks and the Formation of Various High Molecular Weight Complexes in DNA Duplexes. Pyrene-conjugated and nonconjugated TFOs were analyzed for their ability to induce sequence-specific DNA damage on duplex substrates. TFOs (100 nM) or the appropriate controls were incubated with substrates (2 nM), 71*/72* or TA1*/TA2*, for 15 h to allow for triplex formation under equilibrium conditions and subsequently irradiated with a frequency-tripled Nd:YAG laser (355 nm, 84 J). Immediately following irradiation, the samples were subjected to denaturing polyacrylamide gel electrophoresis (PAGE) to assay for damage to the DNA substrates. Figure 2 shows the results obtained using the TA1*/TA2* substrate. Upon irradiation, both specific TFOs, pyr-TC6 and pyr-TC9, induced significant amounts of DNA damage in the form of DNA strand breaks and several high molecular weight products (lanes 8 and 10). The products arising from the DNA strand breaks after irradiation from the 37 bp TA1*/TA2* duplex substrate (labeled on its 5′ ends) were 4−15 and 22−33 bp in size. No damage was observed in samples not subjected to irradiation (odd numbered lanes), in irradi-

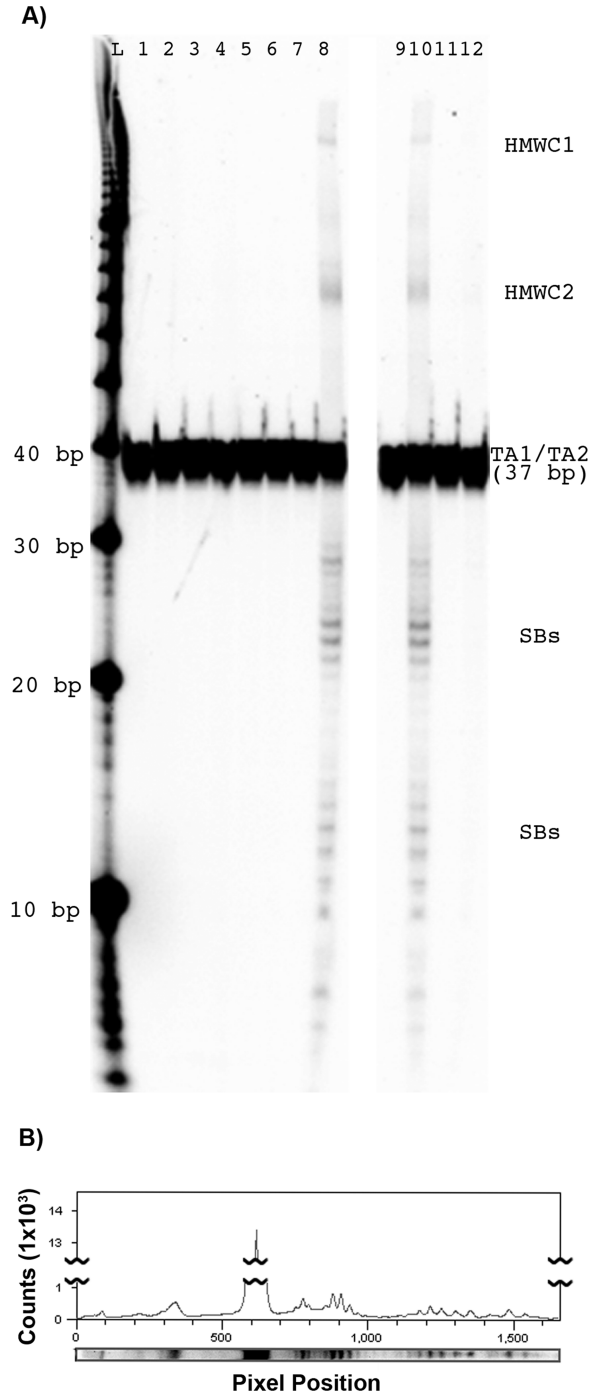

FIGURE 2: Pyrene-conjugated TFOs, pyr-TC6 and pyr-TC9, induce sequence-specific DNA damage on targeted duplex substrates. (A) A 37 bp fragment derived from intron 1 of the hamster *Aprt* gene was labeled on the 5′ end of both strands to create the TC6/9 target substrate, TA1*/TA2*. Samples were analyzed for damage before irradiation (odd numbered lanes) and after irradiation at 355 nm (even numbered lanes). All samples contained TA1*/TA2* (2 nM) in addition to the following: lanes 1 and 2, DNA duplex substrate only; lanes 3 and 4, 100 nM pyrene; lanes 5 and 6, 100 nM TC6; lanes 7 and 8, 100 nM pyr-TC6; lanes 9 and 10, 100 nM py-TC12; lanes 11 and 12, 100 nM pyr-Tscr. Lanes shown were taken from different gels run under identical conditions. Types of DNA damage observed include HMWC1 and HMWC2, which are likely covalent pyrene−DNA adducts, and DNA strand breaks (SBs). Lane L is a 10 bp ladder as a size marker. (B) Example of a densitometric graph, depicting the counts per pixel of lane 8.

Table 2: Yields, Efficiencies, and Effects of Scavengers on Photoinduced DNA Damage by Pyr-TFOs

	damage composition[a] (%)	yields of damage[b] (%)	inhibition[c] (%)		
			KI	D-mannitol	NaN_3
HMWC1	3.5 (±0.5)	0.4/0.6	−25.5	no effect	−34.7
HMWC2	14.9 (±1.4)	1.3/3.1	−34.6	no effect	−41.1
SBs	81.6 (±1.6)	7.7/17.2	−31.7	no effect	−40.8

[a] Percentages reflect the amount of HMWC1, HMWC2, and DNA strand breaks (SBs) with respect to total DNA damage accrued after irradiation at incident energies of 14−420 J. [b] Yields of the three types of damage after minimum (14 J) and maximum (420 J) incident energies at 355 nm. [c] Percent inhibition of DNA damage in samples containing 50 mM KI, D-mannitol, or NaN_3.

ated samples containing the unmodified TFO, TC6 (lane 6), or in samples containing no TFO (lane 2). When the duplex substrate was irradiated in the presence of 100 nM free pyrene (1-pyrenebutanoic acid succinimidyl ester), DNA damage was not detected (lane 4), though the poor solubility of this compound in water may have suppressed its genotoxicity. The TC6- and TC9-directed binding site of pyrene is expected to be 8 and 29 bp from the 5′ ends of TA1* and TA2*, respectively (Figure 1). The data, therefore, suggest that the pyrene moiety is directed to its expected binding site and, upon irradiation, induces strand breaks within ∼7 bp of the target site. Some nonspecific DNA damage was detected in irradiated samples containing 100 nM control TFO, pyr-Tscr (lane 12), but the level of damage was far lower than that observed for the specific TFOs, pyr-TC6 and pyr-TC9.

The results observed for irradiated samples containing pyr-TC6 or pyr-TC9 bound to TA1*/TA2* (the *Aprt* target duplex) were very similar to those obtained from irradiated samples containing the 57 bp 71*/72* *supF* duplex substrate bound by pyr-AC6 or pyr-AC12 TFOs (data not shown). High molecular weight complexes and products of DNA strand breaks, ranging from 12 to 22 and 35 to 45 bp in apparent size, were observed in irradiated samples containing pyr-AC6 and pyr-AC12. The control samples with the pyrene-modified TFO of scrambled sequence had only a small amount of nonspecific damage, similar to what would be expected for low levels of free pyrene. The AC6- and AC12-directed binding sites for the pyrene moiety are expected to be 17 and 40 bp from the 5′ ends of the 71/72 target duplex, respectively (Figure 1). Thus, like the experiments involving pyr-TC6 or TC9, it appears that pyrene is directed by the TFOs to the target duplex substrate and induces DNA strand breaks within ∼5 bp of its expected binding site. Experiments performed with substrates labeled on only one strand or the other (TA1*/TA2, TA1/TA2*, 71*/72, and 71/72*, denoted by asterisk) gave rise to strand breaks, consistent with the notion that both strands are cleaved at or near the expected binding site (data not shown). For example, upon irradiation of samples containing pyr-AC6 or pyr-AC12 and 71*/72, DNA strand breaks gave rise to products ranging from 12 to 22 bp, whereas when the 71/72* was used as the substrate, DNA strand breaks gave rise to products of 35−45 bp.

These results establish that targeted DNA strand breaks are indeed induced by pyrene-TFOs. However, two high molecular weight species (HMWC1 and HMWC2) were also detected after irradiation (Figure 2). A possible explanation is that those products could be adducts of duplex substrate covalently linked to the TFOs through attached pyrene molecules. To test this possibility, we irradiated samples containing unlabeled substrate (TA1/TA2, 1 μM) and ^{32}P-labeled pyr-TC6 (pyr-TC6*, 100 nM) and analyzed by denaturing PAGE. A significant amount of products (∼10% of total signal) with the mobilities of HMWC1 and HMWC2 were observed in irradiated samples only. These results support the notion that HMWC1 and HMWC2 are covalently linked complexes between molecules of pyr-TFOs and their corresponding DNA substrates.

Efficiency of DNA Adduct Formation and Strand Cleavage by Pyr-TFOs. To analyze the kinetics of cleavage and the competing process of photodestruction of the pyrene moiety, we first determined the effectiveness of bleaching of the pyrene chromophore (data not shown). We irradiated 0.1 mM 1-pyrenebutanoic acid succinimidyl ester in 50% DMF with incident energies ranging from 42 to 168 J (30−120 s, 1.4 J/s at 355 nm) and then measured the absorbance of pyrene (E_{335} = 54000 M^{-1} cm^{-1}). The results indicated that the pyrene chromophore is destroyed at a rate of 0.15 J^{-1}. We next sought to identify the yields of the different types of damage with respect to the incident energy (Table 2). Samples containing pyr-AC6 and the 71*/72* *supF* duplex target were irradiated with incident energies ranging from 14 to 420 J (20−300 s, 0.7−1.4 J/s at 355 nm), and the bands corresponding to HMWC1 and HMWC2 and those resulting from single-strand DNA breaks were quantified. The data show a dose-dependent accumulation of HMWC1, HMWC2, and DNA strand breaks associated with a decrease in the amount of undamaged DNA substrate. Maximum yields (i.e., 0.6% HMWC1, 3.1% HMWC2, and 17.2% DNA strand breaks) were generated when samples were irradiated with a total incident energy of 420 J. At both low (0.7 W) and high (1.4 W) power levels, production of strand breaks over time was biphasic, with a rapid phase reaching near-maximal product formation (70%−80%) within 20 s, followed by a slower increase on a time scale of minutes (data not shown). Across all incident energies the composition of DNA damage remained fairly constant and consisted of approximately 3.5% (±0.5) HMWC1, 14.9% (±1.4) HMWC2, and 81.6% (±1.6) DNA strand breaks (Table 2).

The effects of pyr-TFO linker length on the yields and/or the predominant site(s) of DNA damage were also determined. Samples containing pyr-TFOs and their respective substrates were irradiated identically (168 J at 355 nm) and then subjected to denaturing PAGE. Product quantification identified the yields of HMWC1, HMWC2, and the individual products resulting from DNA strand breaks. Pyr-TFOs with longer linkers, pyr-TC9 and pyr-AC12, were slightly less effective than pyr-TC6 or pyr-AC6 at inducing DNA strand breaks and in forming the complexes, HMWC1 and HMWC2. Likewise, the length of the linker separating the pyrene molecule and the TFO had only a modest effect on the position of DNA strand cleavage. The yields of observed DNA strand cleavage induced by pyr-AC6, pyr-AC12, pyr-TC6, or pyr-TC9 at each site are shown in Figure 3. The predominant positions of cleavage within the 71/72 target duplex by both pyr-AC6 and pyr-AC12 were 17 and 40 bp from the 5′ ends of 71 and 72, respectively (Figure 3A, position 0). TFOs AC6 and AC12 bind to their duplex target in an antiparallel orientation, which places their 3′ ends at 17 and 40 bp from the 5′ ends of 71 and 72, respectively.

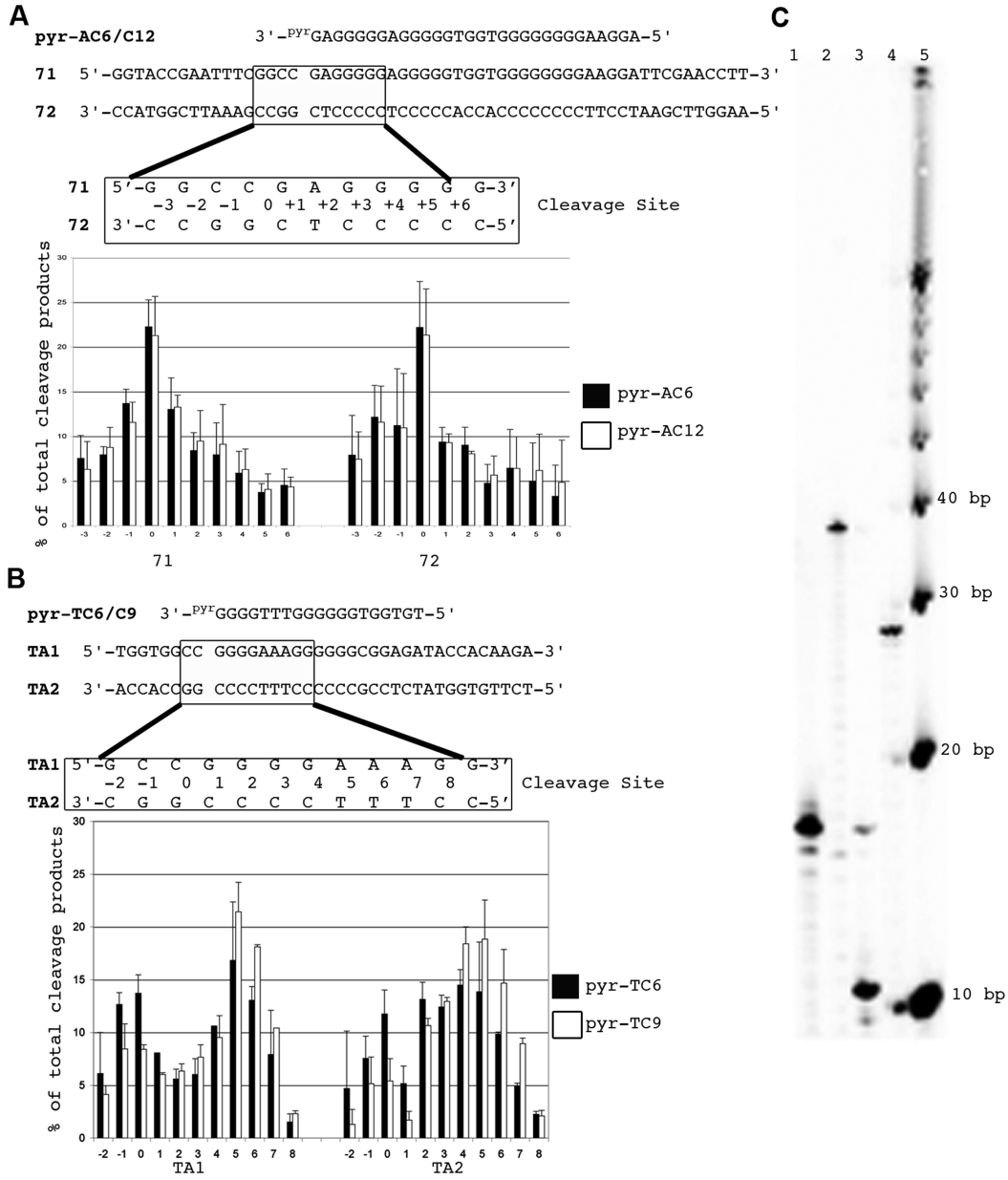

FIGURE 3: Preferential sites of photoinduced DNA strand breaks by pyrene-conjugated TFOs at 100 nM. Shown are the proposed binding configurations of pyr-TFOs to their corresponding target duplex substrates, along with graphs representing the percentage of individual DNA strand break products. For both TFO target sites, pyrene (pyr) was attached to the 3′ ends of the TFOs and is shown to be in close vicinity of cleavage position 0. (A) For pyr-AC6 and pyr-AC12 the preferential site of cleavage is at position 0 within the *supF* duplex target, 71/72. (B) Pyr-TC6 and pyr-TC9 were observed to cleave predominately at positions 0 and 5 within the *Aprt* duplex target, TA1/TA2. (C) The sites of pyr-TFO-induced cleavage of 71, 72, TA1, and TA2 were determined by comparing the mobility of strand break products to that of SSB1 (lane 1), SSB2 (lane 2), SSB3 (lane 3), and SSB4 (lane 4). All experiments were performed in triplicate, and the standard deviations are represented as error bars.

Because pyrene was conjugated to the 3′ ends of those TFOs, the pyrene moiety would be expected to bind in that region and induce DNA damage locally, which appears to be the case for pyr-AC6 and pyr-AC12. The pyr-TFOs targeted to the TA1/TA2 *Aprt* target duplex substrate appear to be less specific at inducing DNA strand breaks (Figure 3B). The proposed binding configuration of pyr-TC6 and pyr-TC9 should align the pyrene molecule 8 and 29 bp from the 5′ ends of TA1 and TA2, respectively (Figure 3B, position 0). While significant cleavage (∼10−15% of total DNA strand breaks) was observed at position 0, the preferential site of cleavage (∼20% of total DNA strand breaks) by pyr-TC6 and pyr-TC9 was position 5, or 13 and 24 bp from the 5′ ends of TA1 and TA2, respectively. In an attempt to understand the observed differences in specificities between the two TFO target sites, we irradiated samples containing pyr-TC6 at a lower concentration (10 nM), which revealed that the preferential site of cleavage (>30% of total damage) shifted to position 0 (data not shown).

The observation that the length of the pyrene-TFO linker had little effect on the efficiency and specificity of cleavage suggests that the pyrene moiety may recognize structural aspects induced by the triplex-duplex junction. In an effort to address this, we irradiated samples containing free pyrene in the presence or absence of TFO (Supporting Information Figure 2). The addition of the unmodified TFO did not appear to result in pyrene-induced DNA damage, indicating that the

triplex-duplex junction did not facilitate pyrene cleavage in the absence of its covalent linkage to the TFO.

Effect of Scavengers on Photoinduced DNA Damage by Pyr-TFOs. Because the mechanism of pyrene-induced photoadduct formation and DNA strand cleavage by 1-hydroxypyrene was previously suggested to be mediated by singlet oxygen and the excited singlet state of pyrene (*43*), we investigated whether a similar mechanism might account for the DNA damage formation reported here when pyrene is conjugated to TFOs. Samples were irradiated in the presence of several radical scavengers (Table 2). NaN_3 is a singlet oxygen scavenger (*44*), and KI is an excited singlet state quencher (*45*), whereas D-mannitol inhibits the formation of hydrogen peroxide and hydroxyl free radicals (*46*). Addition of D-mannitol did not appear to inhibit pyr-TFO-induced DNA damage. However, KI and NaN_3 were both effective at inhibiting the formation of both DNA strand breaks (−32% to −41%) and high molecular weight complexes (−26% to −41%). While these data suggest that singlet oxygen and the excited singlet state of pyrene are crucial for DNA damage induced by pyr-TFOs, whether the same or different mechanisms produce covalent adducts and strand breaks remains to be determined.

Targeted Pyr-TFO-Induced DNA Damage Enhances Mutagenesis, Largely via Deletions. To determine the biological consequence(s) of pyr-TFO-induced DNA damage, mutation frequencies and spectra resulting from the mammalian repair and replication of the damage were determined. The pSupFG1 mutation-reporter shuttle vector, which contains a single binding site for AC6 within the *supF* reporter gene, was irradiated in the presence or absence of pyr-AC6 or pyr-Ascr. Irradiated and nonirradiated samples were allowed to replicate and process the damage for 72 h in mammalian COS-7 cells. Then the plasmids were extracted from the mammalian cells, and *supF* mutation frequencies and spectra were determined as described in the Experimental Procedures section. Interestingly, plasmids irradiated in the presence of pyr-AC6 showed an ~4-fold increase in mutation frequency compared to nonirradiated plasmids under the same conditions and an ~7-fold increase above the background or spontaneous mutation frequency (Figure 4A). Samples irradiated in the presence of the control TFO (pyr-Ascr) or no TFO showed only slightly elevated mutation frequencies (1.2−1.3-fold) compared to the respective nonirradiated samples. Nonirradiated samples treated with pyr-Ascr and pyr-AC6 displayed similar mutation frequencies (1.5−1.7-fold over background), suggesting that the pyrene moiety attached to the TFOs was largely responsible for the induced mutagenesis.

The increase in mutation frequency in irradiated samples treated with pyr-AC6 was apparently due to an increase in deletions, as suggested by the mutation spectra induced by the pyr-TFOs (Figure 4B). A total of nine mutants, three from each experimental condition, were sequenced. Of the samples irradiated in the presence of pyr-AC6, five mutants contained large deletions that included the entire pyr-AC6 binding site. This represented a 150% increase in large deletions compared to the nonirradiated sample under otherwise identical conditions.

DISCUSSION

In the work presented here we provide evidence that pyrene-conjugated TFOs can inflict DNA damage onto their respective target duplexes while maintaining the high affinity and sequence-specific binding properties of the TFOs (Table 1, Figures 2 and 3). We found that, when conjugated to TFOs, pyrene had only moderate effects on binding affinity and specificity. This is intriguing, given another report that suggests substitution of internal nucleotides for a pyrene derivative increases melting temperature of twisted intercalating nucleic acids (TINAs) (*47*). The apparent binding affinities reported here for pyr-TFOs and nonconjugated TFOs (Supporting Information Figure 1) AGRee well with our previous work on similar TFOs that bind to the *supF* or *Aprt* TFO duplex target sites (*14, 19, 39–42*). There are several published reports of the ability of pyrene-based compounds to induce DNA strand breaks and/or adducts (*28–38*). Geacintov et al. (*38*) and Li et al. (*37*) demonstrated photoinduced DNA strand cleavage in samples containing double-stranded oligonucleotides with pyrene adducts. This approach to incorporate pyrene-labeled oligonucleotides into duplexes by annealing would not be applicable to chromosomal targets in cells, and so we have targeted pyrene-mediated photocleavage to defined regions of duplex DNA by addition of pyr-TFOs.

Upon irradiation of samples containing pyr-TFOs bound to their respective duplex substrates, we observed damage in the form of DNA strand breaks and multiple high molecular weight complexes (Figure 2). While we do not know the exact structures of the two high molecular weight complexes HMWC1 and HMWC2, our studies suggest they are covalently linked complexes between strands of the duplex substrate and the pyr-TFOs. The DNA strand breakage observed occurs within 5−7 bp of the expected TFO-directed pyrene-binding site on both strands of the two substrates employed (Figures 2 and 3). The data provide evidence that both strands of the duplex are cleaved. Whether both strands are cut simultaneously remains to be determined; however, pyr-TFOs were observed to linearize a significant amount (up to ~5%) of closed circular plasmids containing their corresponding binding sites only when subjected to irradiation (data not shown), suggesting that the pyr-TFOs may induce DSBs.

Approximately 21% of the targeted substrate was converted to either HMWC1 and HMWC2 (4%), or to DNA strand breaks (17%) by photoreactive pyr-TFOs. Higher yields of DNA damage may be obtainable by altering the chromophore structure or linker in ways that enhance the desired cleavage reactions and reduce competing reactions that occur both for free pyrene and triplex-targeted pyrene. Our findings supporting a role for singlet excited states suggest that chemical modification of the pyrene moiety leading to a reduction in intersystem crossing from singlet to triplet states may be able to bring about an increase in cleavage efficiency. The effect of the linker length between the TFO and the pyrene moiety on the efficiency and specificity of DNA damage generated by pyr-TFOs was also investigated. Our results suggested that pyr-TFOs with shorter linkers (i.e., 6 carbons) were somewhat more specific and efficient at inducing DNA damage than their longer counterparts (of 9 and 12 carbons). These differences may

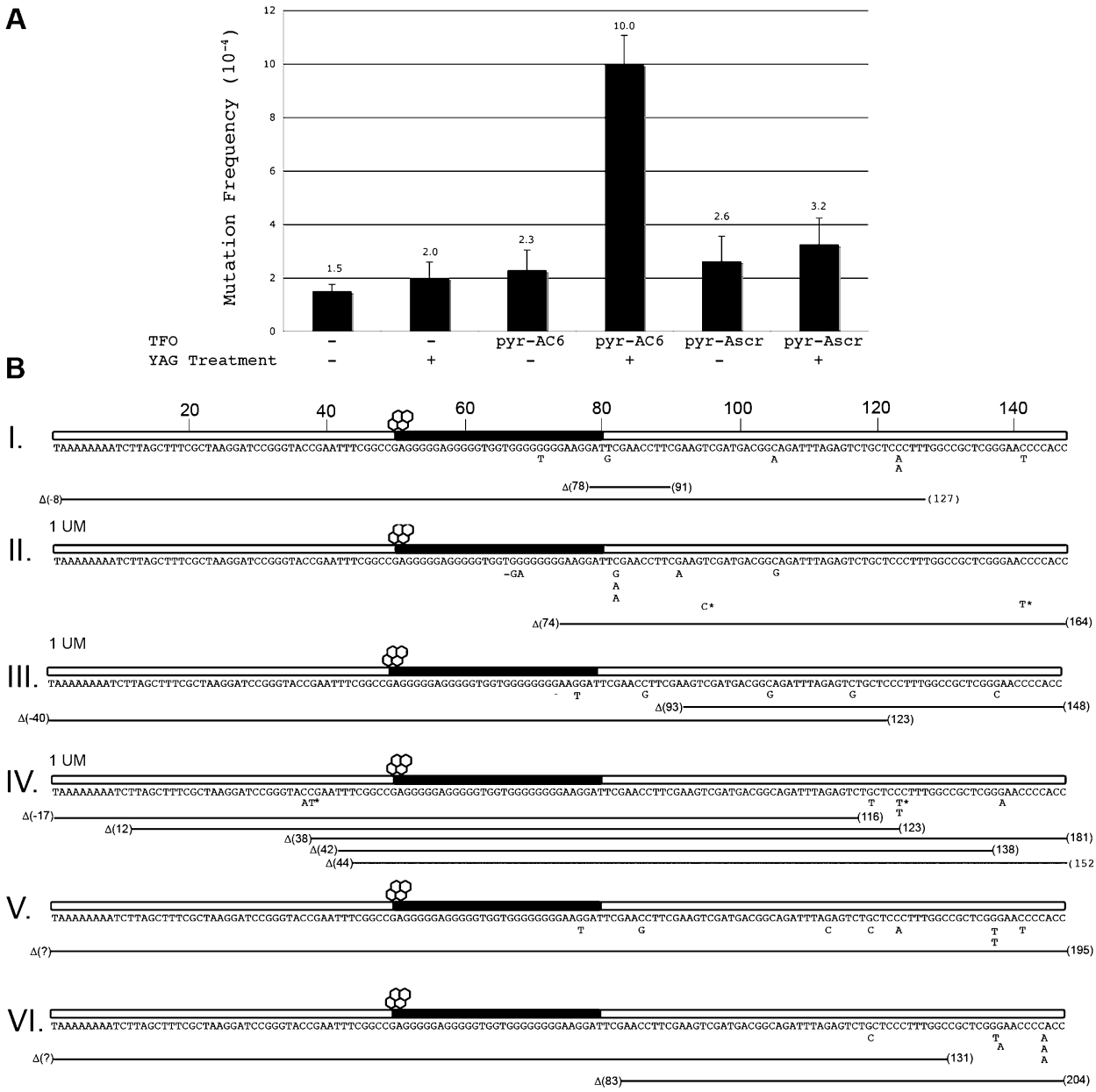

FIGURE 4: Repair of pSupFG1 plasmids containing pyr-AC6-induced DNA damage results in an increase in deletion mutations. pSupFG1 plasmids were irradiated in the presence or absence of pyr-AC6 or pyr-Ascr and allowed replication and repair in COS-7 cells, and mutation frequencies and spectra were determined as described in Experimental Procedures. (A) *SupF* mutation frequencies resulting from repair of the pSupFG1 plasmid in COS-7 cells. Standard deviations from three trials are depicted as error bars. (B) *SupF* mutation spectra resulting from repair of the pSupFG1 plasmid in COS-7 cells: I and II, nonirradiated and irradiated pSupFG1; III and IV, nonirradiated and irradiated pSupFG1 + pyr-AC6; V and VI, nonirradiated and irradiated pSupFG1 + pyr-Ascr. Where designated, UM indicates that no mutation was found within the area sequenced.

be due to orientation, location, and/or steric constraints placed on the pyrene molecule once intercalated into the duplex substrate. Therefore, modifications to the pyrene/TFO linker lengths may yield higher levels of pyr-TFO-induced DNA damage.

The two TFOs used in this study exhibited different preferences for their major sites of DNA strand cleavage at 100 nM. While pyr-AC6 and pyr-AC12 cleaved preferentially at the expected binding site of pyrene, pyr-TC6 and pyr-TC9 induced a substantial amount of cleavage 5 bp downstream of the targeted site (Figure 3). At 10 nM, the preferential site of cleavage by pyr-TC6 shifted to position 0. Thus, differences in specificity and efficiency of the pyr-TFOs can be attributed to concentration, sequence context, and length of the TFO. It seems advisable to use pyr-TFO concentrations less than 100 nM to minimize nonspecific DNA damage. It is important to note that the scrambled pyr-TFOs, pyr-Tscr and pyr-Ascr, did induce low, but detectable levels of DNA damage at 100 nM, consistent with the mobilities of HMWC1 and HMWC2, and what appear to be nonspecific DNA strand breaks. The damage induced by pyr-Tscr and pyr-Ascr was substantially less efficient and specific compared to pyr-TC6, pyr-TC9, pyr-AC6, and pyr-AC12. These results are consistent with detection of low levels of binding by pyr-Tscr and pyr-Ascr at concentrations of 5 μM and previous observations that pyrene-based compounds can induce DNA damage at concentrations as low as 100 nM (*43*).

To investigate the mechanism(s) of DNA damage induced by pyr-TFOs, we irradiated samples in the presence of

various scavengers (Table 2). D-Mannitol, an inhibitor of damage by hydrogen peroxide and hydroxyl radicals, did not appear to impact the type or efficiency of photoinduced DNA damage. However, KI and NaN_3, which are quenchers of excited singlet states and singlet oxygen, respectively, significantly inhibited both formation of HMWC1 and HMWC2 (−26% to −41%) and DNA strand cleavage (−32% to −41%). Similar levels of inhibition by KI (−67%) and NaN_3 (−43%) of photoinduced strand cleavage by 1-hydroxypyrene have been reported previously (*43*). Given past and present evidence on the mechanism of photoinduced DNA damage (*37, 38, 43, 48, 49*), it is apparent that photoexcitation of pyrene to its excited singlet state can have one of two effects aside from degradation. The excited pyrene molecule could either oxidize DNA to form pyrene-DNA adducts or produce local free radicals (i.e., singlet oxygen), both of which could eventually result in DNA strand breaks. While it is evident from the results presented here that singlet oxygen and the excited singlet state of pyrene are involved, the exact mechanisms of DNA strand cleavage and adduct formation induced by pyr-TFOs remain to be identified. Understanding the mechanism of photodamage may help in the design of modifications of pyrene to improve cleavage efficiency.

Mammalian *in vivo* replication and repair of pyr-TFO-induced DNA damage resulted in mutation frequencies ∼4−7-fold above background levels. Over half of the mutants sequenced were found to contain deletions encompassing the entire TFO binding site, suggesting that pyr-TFOs can be targeted to specific sequences on plasmid DNA and induce mutations after processing in mammalian cells. However, because the expected binding site of pyrene within the pSupFG1 plasmid is slightly upstream of the region encoding the *supF* reporter gene, the actual mutation frequency resulting from pyr-TFO-induced DNA damage is likely higher. Furthermore, the possibility exists that some damage was left unrepaired such that the plasmid DNA containing damage did not undergo a full round of DNA replication. Due to the design of our assay, nonreplicated plasmid DNA does not contribute to the mutation frequency or spectrum. All other mutations were found to be single or double base substitutions within the *supF* gene. No trend could be established regarding the point mutations identified within the mutants from all samples. The persistence of an elevated level of large deletions within the region targeted by pyr-TFOs in our experiments is consistent with the error-prone processing of DSBs. Though it cannot be determined from the current data, DSBs could be induced either directly by the pyr-TFOs or indirectly as a result of other biological events (e.g., DNA replication) acting on the DNA containing the pyrene-DNA adducts.

Although it will be desirable to improve the efficiency with which site-selective strand breaks are produced, the current generation of pyr-TFOs already represents powerful tools for directing this kind of damage to target sites in duplex DNA. A very wide range of sequences can be targeted with TFOs, and virtually every mammalian gene contains potential TFO target sites (*50, 51*). The induction of cleavage by light allows exquisite spatial and temporal control of the production of DNA strand breaks and may prove to be highly useful for research purposes that seek to examine DNA repair mechanisms or to modify mammalian genomes.

ACKNOWLEDGMENT

We thank Ms. Sarah Henninger for manuscript preparation and Dr. Richard Wood for discussions and comments.

SUPPORTING INFORMATION AVAILABLE

Two figures as described in the text. This material is available free of charge via the Internet at http://pubs.acs.org.

REFERENCES

1. Fox, K. R., and Brown, T. (2005) An extra dimension in nucleic acid sequence recognition. *Q. Rev. Biophys. 38*, 311–320.
2. Rogers, F. A., Lloyd, J. A., and Glazer, P. M. (2005) Triplex-forming oligonucleotides as potential tools for modulation of gene expression. *Curr. Med. Chem. Anticancer Agents 5*, 319–326.
3. Besch, R., Giovannangeli, C., and Degitz, K. (2004) Triplex-forming oligonucleotides—sequence-specific DNA ligands as tools for gene inhibition and for modulation of DNA-associated functions. *Curr. Drug Targets 5*, 691–703.
4. Panyutin, I. G., Sedelnikova, O. A., Karamychev, V. N., and Neumann, R. D. (2003) Antigene radiotherapy: targeted radiodamage with ^{125}I-labeled triplex-forming oligonucleotides. *Ann. N.Y. Acad. Sci. 1002*, 134–140.
5. Nagatsugi, F., and Sasaki, S. (2004) Chemical tools for targeted mutagenesis of DNA based on triple helix formation. *Biol. Pharm. Bull. 27*, 463–467.
6. Vasquez, K. M., and Wilson, J. H. (1998) Triplex-directed modification of genes and gene activity. *Trends Biochem. Sci. 23*, 4–9.
7. Vasquez, K. M., and Glazer, P. M. (2002) Triplex-forming oligonucleotides: principles and applications. *Q. Rev. Biophys. 35*, 89–107.
8. Vasquez, K. M., Marburger, K., Intody, Z., and Wilson, J. H. (2001) Manipulating the mammalian genome by homologous recombination. *Proc. Natl. Acad. Sci. U.S.A. 98*, 8403–8410.
9. Nagatsugi, F., Kawasaki, T., Tokuda, N., Maeda, M., and Sasaki, S. (2001) Site-directed alkylation to cytidine within duplex by the oligonucleotides containing functional nucleobases. *Nucleosides, Nucleotides, Nucleic Acids 20*, 915–919.
10. Povsic, T. J., and Dervan, P. B. (1990) Sequence-specific alkylation of double-helical DNA by oligonucleotide-directed triple-helix formation. *J. Am. Chem. Soc. 112*, 9428–9430.
11. Reed, M. W., Lukhtanov, E. A., Gorn, V., Kutyavin, I., Gall, A., Wald, A., and Meyer, R. B. (1998) Synthesis and reactivity of aryl nitrogen mustard-oligodeoxyribonucleotide conjugates. *Bioconjugate Chem. 9*, 64–71.
12. Shaw, J.-P., Milligan, J. F., Krawczyk, S. H., and Matteucci, M. (1991) Specific, high-efficiency, triple-helix-mediated cross-linking to duplex DNA. *J. Am. Chem. Soc. 113*, 7765–7766.
13. Takasugi, M., Guendouz, A., Chassignol, M., Decout, J. L., Lhomme, J., Thuong, N. T., and Helene, C. (1991) Sequence-specific photo-induced cross-linking of the two strands of double-helical DNA by a psoralen covalently linked to a triple helix-forming oligonucleotide. *Proc. Natl. Acad. Sci. U.S.A. 88*, 5602–5606.
14. Vasquez, K. M., Wensel, T. G., Hogan, M. E., and Wilson, J. H. (1996) High-efficiency triple-helix-mediated photo-cross-linking at a targeted site within a selectable mammalian gene. *Biochemistry 35*, 10712–10719.
15. Perkins, B. D., Wensel, T. G., Vasquez, K. M., and Wilson, J. H. (1999) Psoralen photo-cross-linking by triplex-forming oligonucleotides at multiple sites in the human rhodopsin gene. *Biochemistry 38*, 12850–12859.
16. Puri, N., Majumdar, A., Cuenoud, B., Miller, P. S., and Seidman, M. M. (2004) Importance of clustered 2′-O-(2-aminoethyl) residues for the gene targeting activity of triple helix-forming oligonucleotides. *Biochemistry 43*, 1343–1351.
17. Puri, N., Majumdar, A., Cuenoud, B., Natt, F., Martin, P., Boyd, A., Miller, P. S., and Seidman, M. M. (2002) Minimum number of 2′-O-(2-aminoethyl) residues required for gene knockout activity by triple helix forming oligonucleotides. *Biochemistry 41*, 7716–7724.
18. Majumdar, A., Puri, N., Cuenoud, B., Natt, F., Martin, P., Khorlin, A., Dyatkina, N., George, A. J., Miller, P. S., and Seidman, M. M. (2003) Cell cycle modulation of gene targeting by a triple helix-forming oligonucleotide. *J. Biol. Chem. 278*, 11072–11077.

19. Vasquez, K. M., Narayanan, L., and Glazer, P. M. (2000) Specific mutations induced by triplex-forming oligonucleotides in mice. *Science 290*, 530–533.
20. Mezhevaya, K., Winters, T. A., and Neumann, R. D. (1999) Gene targeted DNA double-strand break induction by (125)I-labeled triplex-forming oligonucleotides is highly mutagenic following repair in human cells. *Nucleic Acids Res. 27*, 4282–4290.
21. Panyutin, I. G., and Neumann, R. D. (1994) Sequence-specific DNA double-strand breaks induced by triplex forming ^{125}I labeled oligonucleotides. *Nucleic Acids Res. 22*, 4979–4982.
22. Sedelnikova, O. A., Panyutin, I. V., Neumann, R. D., Bonner, W. M., and Panyutin, I. G. (2004) Assessment of DNA damage produced by ^{125}I-triplex-forming oligonucleotides in cells. *Int. J. Radiat. Biol. 80*, 927–931.
23. Pei, D., Corey, D. R., and Schultz, P. G. (1990) Site-specific cleavage of duplex DNA by a semisynthetic nuclease via triple-helix formation. *Proc. Natl. Acad. Sci. U.S.A. 87*, 9858–9862.
24. Eisenschmidt, K., Lanio, T., Simoncsits, A., Jeltsch, A., Pingoud, V., Wende, W., and Pingoud, A. (2005) Developing a programmed restriction endonuclease for highly specific DNA cleavage. *Nucleic Acids Res. 33*, 7039–7047.
25. Moser, H. E., and Dervan, P. B. (1987) Sequence-specific cleavage of double helical DNA by triple helix formation. *Science 238*, 645–650.
26. Perrouault, L., Asseline, U., Rivalle, C., Thuong, N. T., Bisagni, E., Giovannangeli, C., Le Doan, T., and Helene, C. (1990) Sequence-specific artificial photo-induced endonucleases based on triple helix-forming oligonucleotides. *Nature 344*, 358–360.
27. Teulade-Fichou, M. P., Perrin, D., Boutorine, A., Polverari, D., Vigneron, J. P., Lehn, J. M., Sun, J. S., Garestier, T., and Helene, C. (2001) Direct photocleavage of HIV-DNA by quinacridine derivatives triggered by triplex formation. *J. Am. Chem. Soc. 123*, 9283–9292.
28. Toyooka, T., Ibuki, Y., Takabayashi, F., and Goto, R. (2006) Coexposure to benzo[a]pyrene and UVA induces DNA damage: first proof of double-strand breaks in a cell-free system. *Environ. Mol. Mutagen. 47*, 38–47.
29. Toyooka, T., Ibuki, Y., Koike, M., Ohashi, N., Takahashi, S., and Goto, R. (2004) Coexposure to benzo[a]pyrene plus UVA induced DNA double strand breaks: visualization of Ku assembly in the nucleus having DNA lesions. *Biochem. Biophys. Res. Commun. 322*, 631–636.
30. Feng, T., Guo, X. Q., Zheng, W. Y., and Yuan, D. X. (2003) Detection of DNA strand breaks in the liver of *Boleophthalmus pectinirostris* treated with benzo(a)pyrene. *Bull. Environ. Contam. Toxicol. 71*, 263–269.
31. Ching, E. W., Siu, W. H., Lam, P. K., Xu, L., Zhang, Y., Richardson, B. J., and Wu, R. S. (2001) DNA adduct formation and DNA strand breaks in green-lipped mussels (*Perna viridis*) exposed to benzo[a]pyrene: dose- and time-dependent relationships. *Mar. Pollut. Bull. 42*, 603–610.
32. Routledge, M. N., McLuckie, K. I., Jones, G. D., Farmer, P. B., and Martin, E. A. (2001) Presence of benzo[a]pyrene diol epoxide adducts in target DNA leads to an increase in UV-induced DNA single strand breaks and supF gene mutations. *Carcinogenesis 22*, 1231–1238.
33. Hanelt, S., Helbig, R., Hartmann, A., Lang, M., Seidel, A., and Speit, G. (1997) A comparative investigation of DNA adducts, DNA strand breaks and gene mutations induced by benzo[a]pyrene and (±)-anti-benzo[a]pyrene-7,8-diol 9,10-oxide in cultured human cells. *Mutat. Res. 390*, 179–188.
34. Vaghef, H., Wisen, A. C., and Hellman, B. (1996) Demonstration of benzo(a)pyrene-induced DNA damage in mice by alkaline single cell gel electrophoresis: evidence for strand breaks in liver but not in lymphocytes and bone marrow. *Pharmacol. Toxicol. 78*, 37–43.
35. Nordenskjold, M., and Jernstrom, B. (1982) Induction and repair of DNA strand breaks in cultured human fibroblasts exposed to various phenols and dihydrodiols of benzo[a]pyrene. *Chem.-Biol. Interact. 41*, 155–168.
36. Nordenskjold, M., Soderhall, S., Moldeus, P., and Jernstrom, B. (1978) Differences in the repair of DNA strand breaks induced by 9-hydroxy-benzo(a)pyrene and trans-7,8-dihydro-7,8-dihydroxy-benzo(a)pyrene in cultured human fibroblasts. *Biochem. Biophys. Res. Commun. 85*, 1535–1541.
37. Li, B., Mao, B., Liu, T. M., Xu, J., Dourandin, A., Amin, S., and Geacintov, N. E. (1995) Laser pulse-induced photochemical strand cleavage of site-specifically and covalently modified (+)-anti-benzo[a]pyrene diol epoxide-oligonucleotide adducts. *Chem. Res. Toxicol. 8*, 396–402.
38. Geacintov, N., Solntsev, K., Johnson, L. W., Chen, J., Kolbanovskiy, A. D., Liu, T., and Shafirovich, V. (1998) Photoinduced electron transfer and strand cleavage in pyrenyl-DNA complexes and adducts. *J. Phys. Org. Chem. 11*, 561–565.
39. Wu, Q., Christensen, L. A., Legerski, R. J., and Vasquez, K. M. (2005) Mismatch repair participates in error-free processing of DNA interstrand crosslinks in human cells. *EMBO Rep. 6*, 551–557.
40. Vasquez, K. M., Dagle, J. M., Weeks, D. L., and Glazer, P. M. (2001) Chromosome targeting at short polypurine sites by cationic triplex-forming oligonucleotides. *J. Biol. Chem. 276*, 38536–38541.
41. Vasquez, K. M., Wensel, T. G., Hogan, M. E., and Wilson, J. H. (1995) High-affinity triple helix formation by synthetic oligonucleotides at a site within a selectable mammalian gene. *Biochemistry 34*, 7243–7251.
42. Reddy, M. C., Christensen, J., and Vasquez, K. M. (2005) Interplay between human high mobility group protein 1 and replication protein A on psoralen-cross-linked DNA. *Biochemistry 44*, 4188–4195.
43. Dong, S., Hwang, H. M., Shi, X., Holloway, L., and Yu, H. (2000) UVA-Induced DNA single-strand cleavage by 1-hydroxypyrene and formation of covalent adducts between DNA and 1-hydroxypyrene. *Chem. Res. Toxicol. 13*, 585–593.
44. Hasty, N., Merkel, P. B., Radlick, P., and Kearns, D. R. (1972) Role of azide in singlet oxygen reaction. Reaction of azide with singlet oxygen. *Tetrahedron. Lett. 13*, 49–52.
45. Miller, J. C., Meek, J. S., and Strickler, S. J. (1977) Heavy atom effects on the triplet lifetimes of naphthalene and phenanthrene. *J. Am. Chem. Soc. 99*, 8175–8179.
46. Goldstein, S., and Czapski, G. (1984) Mannitol as an OH• scavenger in aqueous solutions and in biological systems. *Int. J. Radiat. Biol. Relat. Stud. Phys. Chem. Med. 46*, 725–729.
47. Filichev, V. V., and Pedersen, E. B. (2005) Stable and selective formation of hoogsteen-type triplexes and duplexes using twisted intercalating nucleic acids (TINA) prepared via postsynthetic Sonogashira solid-phase coupling reactions. *J. Am. Chem. Soc. 127*, 14849–14858.
48. Wagenknecht, H. A. (2003) Reductive electron transfer and transport of excess electrons in DNA. *Angew. Chem., Int. Ed. Engl. 42*, 2454–2460.
49. Dunn, D. A., Lin, V. H., and Kochevar, I. E. (1992) Base-selective oxidation and cleavage of DNA by photochemical cosensitized electron transfer. *Biochemistry 31*, 11620–11625.
50. Wu, Q., Gaddis, S. S., MacLeod, M. C., Walborg, E. F., Thames, H. D., DiGiovanni, J., and Vasquez, K. M. (2007) High-affinity triplex-forming oligonucleotide target sequences in mammalian genomes. *Mol. Carcinog. 46*, 15–23.
51. Gaddis, S. S., Wu, Q., Thames, H. D., DiGiovanni, J., Walborg, E. F., MacLeod, M. C., and Vasquez, K. M. (2006) A web-based search engine for triplex-forming oligonucleotide target sequences. *Oligonucleotides 16*, 196–201.

BI7024029